First-principles calculation of shift current bulk photovoltaic effect in two-dimensional α-In₂Se₃

Rajender Prasad Tiwari ⬤, Balaji Birajdar ⬤, and Ram Krishna Ghosh ⬤*
Special Center for Nano Sciences, Jawaharlal Nehru University, New Delhi 110067, India

Shift current is the dominant dc-current response in the bulk photovoltaic effect (BPVE), which is the conversion of solar energy into electricity in the materials with broken inversion symmetry. While the guiding principle of BPVE is a lack of inversion symmetry in a material which also results in ferroelectricity, it is therefore, expected that a significantly large shift current is achieved in ferroelectric materials. In this work, we calculate shift current using first principles in two-dimensional α-In₂Se₃ which has both in-plane and out-of-plane polarization at room temperature. To understand the implications of in-plane and out-of-plane polarization on shift current BPVE, mono- and bilayer structures of 3R and 2H α-In₂Se₃ are considered in our calculations. It suggests that the in-plane polarization doesn't affect the shift current response of this material. In monolayer, a dominant shift current response of magnitude $750\,\mu\mathrm{A/V^2}$ is obtained along the direction of out-of-plane polarization under uniform illumination of zz-polarized light at a photon energy of 4.16 eV. The doping engineering is further implemented to tune the shift current response to visible light. Bismuth (Bi) is used to substitute the indium element at the tetrahedral site thereby introducing more energy levels in the conduction band which importantly are contributed by p orbitals of Bi and take part in the transition process. Consequently, a giant shift current of $1200\,\mu\mathrm{A/V^2}$ is obtained at a photon energy of 2.98 eV. The present study would be an instrumental in understanding the shift current BPVE and would pave the path for designing efficient photovoltaic devices based on α-In₂Se₃ and similar material systems.

I. INTRODUCTION

The conversion of solar energy into electric current in the materials with broken inversion symmetry is called bulk photovoltaic effect (BPVE) [1]. It is a technologically important phenomenon as it can generate a photovoltage more than the band gap of the material [2]. Moreover, its photoconversion efficiency is not limited by the Shockley-Queisser limit unlike the conventional *p-n* junction solar cells [3–5]. Therefore, BPVE is viewed as one of the most efficient alternative sources of green energy. Because of its prospective scope in solar energy harvesting applications, intense research is being done to understand or formulate a mechanism to improve its efficiency. Though the necessary ingredient to optimize the BPVE is still not fully understood, a material with the band gap in visible range (1.1–3.1 eV) [5,6], large electronic densities of states near the band edge, and high anisotropy are beneficial [5,7,8]. The latter ensures a preferential direction of current (called "shift current") flow through such material-based devices under uniform illumination.

The shift current BPVE is a nonlinear optical process that arises from second-order interaction with monochromatic light. Photoexcitation of electrons from one band to another accompanying a coordinate shift allows a net current flow from the asymmetry of the potential resulting in a shift current [3–5]. The shift current is a dominant dc-current response

in BPVE [7] therefore, the shift current and BPVE are used interchangeably in this paper. The shift current tensor is given as [8–11]

$$
\begin{aligned}
\sigma^{abc}&(0;\ \omega,\ -\omega)\\
&= -\frac{i\,\pi e^3}{2\hbar^2}\int [d\boldsymbol{k}]\sum_{n,m} f_{nm}\big(r^b_{mn}r^c_{nm;a} + r^c_{mn}r^b_{nm;a}\big)\\
&\quad\times\ \delta(\omega_{mn} - \omega),
\end{aligned}
\tag{1}
$$

where a, b, c are Cartesian indices, n and m are the band indices, $f_{nm} = f_n - f_m$ is the Fermi-Dirac occupation number, $\omega_{nm} = \omega_n - \omega_m$ is the band energy difference, r^b_{mn} is the dipole matrix elements, $r^b_{nm;a}$ represents generalized derivatives, the integral is over the first Brillouin zone with $[d\boldsymbol{k}] = dk^d/(2\pi)^d$ in d dimensions, and k is the wave vector. The dipole matrix elements are defined as $r^b_{mn} \equiv A^b_{mn}$ when $n \neq m$ or zero otherwise [7]. The term A^b_{mn} is the Berry connection matrix given as $A^b_{mn} = i\langle u_m|\partial_{k_b}|u_n\rangle$, where $|u_n\rangle$ denotes the cell periodic part of a Bloch eigenstate. The generalized derivative is defined as $r^b_{nm;a} = \partial_{k_a} r^b_{nm} - i(A^a_{nn} - A^a_{mm})r^b_{nm}$.

Under a monochromatic light of form $E^b(t) = E^b(\omega)e^{i\omega t} + E^b(-\omega)e^{-i\omega t}$ with frequency ω and linearly polarized along the direction b, the dc-photocurrent density (J) from the linear BPVE is given as [7,10]

$$
J^a_{\text{shift}}(\omega) = 2\sum_b \sigma^{abb}(0;\ \omega,\ -\omega)E^b(\omega)E^b(-\omega)
\tag{2}
$$

*Author to whom correspondence should be addressed: ramki.phys@gmail.com

and the second-order response function for the shift current becomes

$$\sigma^{abb}(0;\ \omega,\ -\omega) = \frac{\pi e^3}{\hbar^2} \int [d\boldsymbol{k}] \sum_{n,m} f_{nm} R_{nm}^{a,b}$$

$$\times\ r_{nm}^b r_{mn}^b \times \delta(\omega_{mn} - \omega), \qquad (3)$$

where $R_{nm}^{a,b}$ is a shift vector [9,10] defined as

$$R_{nm}^{a,b} = \partial_{k_a}\phi_{nm}^b - A_{mm}^a + A_{nn}^a; \qquad (4)$$

here ϕ_{nm}^b is the phase of $r_{nm}^b = |r_{nm}^b|e^{-i\phi_{nm}^b}$. The shift vector $R_{nm}^{a,b}$ has a unit of length and can be physically interpreted as, on average, the displacement of coherent carriers during their lifetimes when they are pumped from band m to band n. According to Fermi's golden rule, the product $r_{nm}^b r_{mn}^b \times \delta(\omega_{nm} - \omega) = |r_{nm}^b|^2\delta(\omega_{nm} - \omega)$ in Eq. (3) can be interpreted as a transition rate from band m to band n. Therefore, the shift current response is expressed as the shift vector multiplied by the transition rate.

BPVE has long been studied intensively in conventional ABO_3 ferroelectric oxides because the fundamental requirement of broken inversion symmetry is well satisfied in such materials. However, in most of such material systems, the bands involved in the transition process are strongly contributed by the localized d orbitals which tend to decrease the shift current [12]. Moreover, studies show that the shift current can be improved by choosing the material systems with a large joint density of states where the band edge is closely aligned with the peak of the solar spectrum [5,12]. Since the band edge always induces a Van Hove singularity in the density of states, the requirement of a large peak in the photoresponse can be naturally better satisfied by low dimensional materials, which generically present stronger singularities [5,7,12]. Therefore, the recent development of a number of two-dimensional (2D) materials with broken inversion symmetry has opened up a new paradigm to the BPVE. Recently, Rangel *et al.* reported a large shift current ($\sim$100 μA/V^2) in single-layer GeS monochalcogenide [8]. Interestingly, the reported shift current in single-layer GeS (thickness $\sim$2.6 Å) is far larger than that in the most studied ferroelectric perovskite oxides such as BaTiO$_3$ (30 μA/V^2), and PbTiO$_3$ (50 μA/V^2) in bulk [4], suggesting that the 2D van der Waals (vdW) layered materials are promising for photovoltaic applications at an ultimate scaling thickness.

The polar 2D vdW materials, especially, are more interesting because a large shift current BPVE is reported in such material systems [12]. Although polarization and shift current are not linked in any specific way despite the fact that both originate from inversion symmetry breaking, it is reported that a material with larger polarization would significantly enhance the bulk photovoltaic response [6,13–15]. The shift current response has been studied in many material systems including perovskite oxides [3,4], organometal-halide perovskites [16], and 2D material system [8,10,11], etc., however, to our knowledge it has been studied in the material systems in which polarization exists in one direction (i.e., either in plane or out of plane). But a recent development in the 2D material system with broken inversion symmetry leads to the emergence of the group III$_2$–VI$_3$ vdW materials which are reported to possess a robust in-plane as well as out-of-plane polarization [17–19].

Understanding the implications of coexisting in-plane and out-of-plane polarization on shift current is, therefore, vital in down selecting the material and designing the photovoltaic devices with improved efficiency. Therefore, in this study, we choose α-In$_2$Se$_3$, a crystalline family member of In$_2$Se$_3$, which is a prototypical 2D layered material system having both in-plane and out-of-plane polarization.

In$_2$Se$_3$ is an intriguing III−VI binary chalcogenide with diverse electronic properties and crystalline polymorphism existing in at least five different crystalline phases, viz., α, β, γ, δ, and κ [20,21]. At room temperature, α-In$_2$Se$_3$ has a hexagonal crystal structure and is a multidirectional ferroelectric layered semiconductor with a robust in-plane and out-of-plane polarization [17,21]. It has been widely studied theoretically and experimentally with the view of its applications in two-dimensional memory and optoelectronics such as photodetectors [22–25]. However, the photovoltaic application of α-In$_2$Se$_3$ is still not well explored. Therefore, here we theoretically study its shift current BPVE application and implications of in-plane and out-of-plane polarization on it. We find that a large BPVE shift current of 750 μA/V^2 is obtained along the direction of out-of-plane polarization and a negligible shift current is obtained along the direction of in-plane polarization direction when illuminated by a zz-polarized and xx/yy-polarized light, respectively. Furthermore, the highest shift current response lies in the ultraviolet range ($\sim$4.16 eV) which can be tuned effectively by doping. Wisely choosing the dopant and doping site, an enhanced shift current ($\sim$1200 μA/V^2) is obtained in single-layer InBiSe$_3$ system that importantly occurs in the visible spectrum range.

II. METHODOLOGY

Density functional theory (DFT) calculations were performed using the QUANTUM ESPRESSO package [26] with the ultrasoft pseudopotential [27] as parameterized by the Perdew-Zunger exchange correlation [28]. The plane-wave basis set with an energy cutoff of 70 Ry and $8 \times 8 \times 1$ Monkhorst-Pack k-point grid was found to optimally converge self-consistent energy up to 10^{-5} Ry using Davidson diagonalization algorithm [29]. Fermi-Dirac distribution with a width of $k_B T = 0.005$ Ry was used for smearing the occupation of numbers of electronic states. A vacuum layer of 20 Å along the Z axis was used to minimize the interactions between the periodic images of the layers. In order to account for vdW interaction, we tested many vdW correction functionals [30,31] and the vdW-df-obk8 functional was used as it defined the lattice constants of this material more accurately. The calculations were sufficiently converged to allow the atomic structures to be optimized until the residual forces on the atoms are less than 10^{-4} Ry/bohr. Uniform k-point grid of $8 \times 8 \times 1$ and $30 \times 30 \times 1$ was used for self-consistent and non-self-consistent calculations, respectively. Polarization was calculated by the quantum theory of polarization approach [32] using Berry's phase method. The hybrid functional Heyd-Scuseria-Ernzerhof-06 (HSE06) [33], as implemented in QuantumATK [34], was used to correctly describe the electronic band structures. Based on HSE06 band-structure calculations, Hubbard U was further optimized using electronic property calculation [6] and used as a basis to
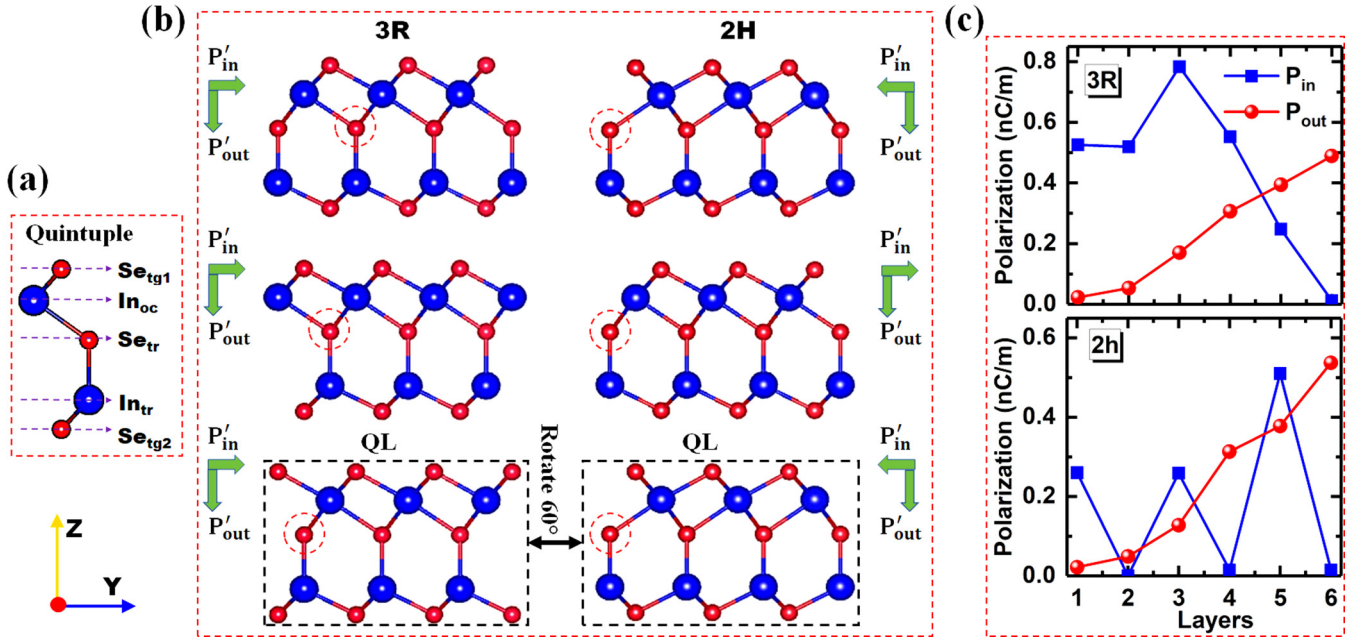
FIG. 1. Showing the side view of an α-In$_2$Se$_3$ quintuple (a); quintuple layers and their stacking in rhombohedral (3R) and hexagonal (2H) arrangement (b); variation of in-plane (P_{in}) and out-of-plane (P_{out}) polarization with the number of layers in these stacking arrangements (c). In a quintuple, the In atoms, In$_{oc}$ and In$_{tr}$ are coordinated octahedrally and tetrahedrally, respectively, while the Se atoms at the top (Se$_{tg1}$) and bottom layer (Se$_{tg2}$) are coordinated trigonally, and the central Se$_{tr}$ atom (encircled) is coordinated tetrahedrally via which the P_{in} and P_{out} in a quintuple layer (QL) are interlinked. The alignment of in-plane polarization (P'_{in}) and out-of-plane polarization (P'_{out}) of the individual layer are also indicated (green arrow).

take into account the correlation effect in Wannier functions in QUANTUM ESPRESSO. Since electronic bands near the Fermi level of In$_2$Se$_3$ are greatly influenced by p orbitals of In and Se, therefore, in order to treat the large self-interaction error originating from p orbitals, an optimum Hubbard U of 4.6 eV was applied on the p orbitals of both In and Se.

Considering the optimized local-density approximation plus Hubbard U (USPP/LDA + U or simply LDA + U unless until specified) Kohn-Sham potential, maximally localized Wannier functions (MLWFs) were created using the Wannier90 code [35] in the slab geometry as obtained after orthogonalizing the hexagonal α-In$_2$Se$_3$. On obtaining MLWFs, the Wannier interpolation method was used to calculate the shift current conductivity using a refined k grid of $200 \times 200 \times 1$ and a boarding factor of 0.04 eV. The k grid of $200 \times 200 \times 1$ was chosen after performing the shift current convergence test with the k points. Furthermore, to check the stability of band structures and the shift current response against the change of pseudopotentials in α-In$_2$Se$_3$, along with the Hubbard U, we used ultrasoft pseudopotential with Perdew, Burke, and Ernzerhof exchange correlation (USPP/GGA + U), and projector-augmented wave parametrized by Perdew-Zunger exchange-correlation functional (PAW/LDA + U). The optimized Hubbard U of 4.8 and 5.0 eV were used with USPP/GGA and PAW/LDA, respectively applied on the p orbitals of both In and Se.

III. RESULTS AND DISCUSSION

Structure of α-In$_2$Se$_3$ — Among the five (α, β, γ, δ, and κ) known crystalline polymorphisms of In$_2$Se$_3$, the α-In$_2$Se$_3$

is a layered 2D semiconductor at room temperature and is a technologically important material system [19–21,24]. Using mechanical or chemical exfoliation, mono to a few layers of α-In$_2$Se$_3$ is easily obtained [21,36]. The building block of α-In$_2$Se$_3$ is a quintuple consisting of Se-In-Se-In-Se atomic sequence connected by the strong covalent bond vertically [Fig. 1(a)]. Similar quintuple layers (QLs) can be stacked stable by the weak out-of-plane vdW interactions. Depending upon the geometrical orientation of stacked quintuple layers, the α-In$_2$Se$_3$ may adopt two different crystal structures: rhombohedral (3R) or hexagonal (2H) [21], as shown in Fig. 1(b). The 3R structure has a three-layered cell unit comprising of identical QLs with a constant translation along the xy plane, belonging to the $R3m$ (no. 160) space group, whereas the 2H structure has a two-layered cell unit with each successive QL rotated by 180° in the xy plane to its preceding QL and it belongs to the $P6_3/mc$ (no. 186) space group. The 3R and 2H structures are easily transferred into each other by turning and moving the layers along the xy plane. An optimized in-plane lattice constant of 4.0751 Å in 3R and 4.0761 Å in the 2H structure is obtained which matches closely the previous reports [17,21] (a lattice constant calculated using different pseudopotentials is shown in Table S1 in the Supplemental Material [37]).

In addition to the enigma of QL stacking in α-In$_2$Se$_3$, the Se and In atoms have different coordination polyhedra. In a quintuple, the Se atoms at the top (Se$_{tg1}$) and bottom layer (Se$_{tg2}$) are coordinated trigonally with In$_{oc}$ and In$_{tr}$, respectively (see Fig. S1 in the Supplemental Material [37]). The In$_{oc}$ on the other hand is coordinated octahedrally by six Se atoms, and the In$_{tr}$ is coordinated tetrahedrally by
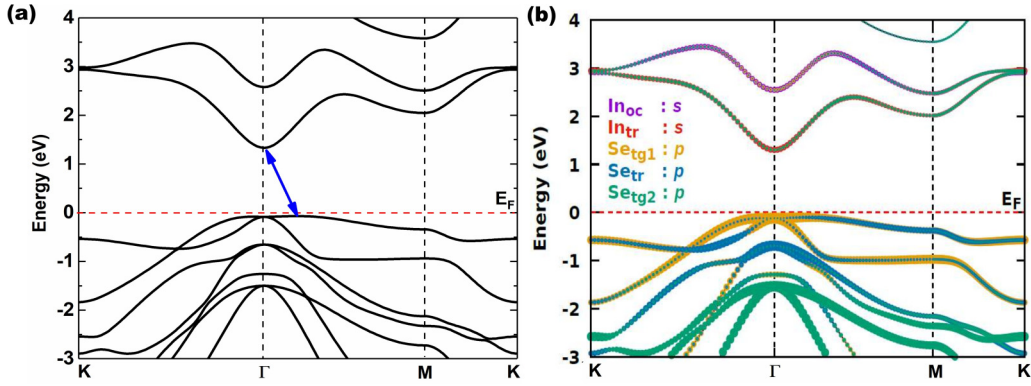
FIG. 2. (a) Electronic band structure of single-layer α-In$_2$Se$_3$ as obtained with LDA $+$ U. It is an indirect band semiconductor with conduction-band minimum (CBM) at the Γ point and the valance-band maximum (VBM) lies between Γ and M points as indicated by an arrow; (b) fat band of single-layer α-In$_2$Se$_3$ showing the contribution of s and p orbitals of In and Se.

four Se atoms, whereas the central Se$_{tr}$ atom is tetrahedrally sandwiched by In$_{oc}$ and In$_{tr}$ atoms. The Se$_{tr}$ atom plays a vital role in persuading the distinguished attribute of coexistence of in-plane and out-of-plane polarization in α-In$_2$Se$_3$. In its low-energy symmetry, the Se$_{tr}$ atom [Fig. 1(a)] undergoes a vertical movement along the Z axis in addition to the lateral movement along the xy plane. Due to its vertical movement, there is a dramatic difference in the bond length between Se$_{tr}$-In$_{oc}$ and Se$_{tr}$-In$_{tr}$ ($\sim$0.36 Å) leading to the breaking of out-of-plane centrosymmetry and hence an out-of-plane polarization (P_{out}) along the Z axis, whereas the lateral movement of Se$_{tr}$ leads to the breaking of in-plane centrosymmetry, resulting in an in-plane polarization (P_{in}) in the xy plane; therefore, P_{in} and P_{out} are interlinked in this material system. In a QL of thickness 6.8 Å, we calculate a robust P_{in} and P_{out} of 0.53 nC/m and 0.023 nC/m, respectively which is quite larger than the previously reported in-plane polarization in γ-SbP (0.38 nC/m) [38] and out-of-plane polarization in γ-LiAlTe$_2$ [39]. Therefore, α-In$_2$Se$_3$ can provide a robust multidirectional polarization at an ultimate scaling length of a few angstroms.

Interestingly, in a multilayer α-In$_2$Se$_3$ system, the strength of polarization depends upon the stacking style of the QL (i.e., $3R$ or $2H$). Variation of P_{out} and P_{in} in $3R$ and $2H$ α-In$_2$Se$_3$ with layers is shown in Fig. 1(c). If the in-plane and out-of-plane polarization of individual layer is represented as P'_{in} and P'_{out} as indicated in Fig. 1(b), then in both $3R$ and $2H$ stacking arrangements, the P'_{out} of each layer is always along the $-z$ (or $+z$) axis, therefore, the total out-of-plane polarization P_{out} gradually increases with the number of layers [40]. The strength of the net in-plane polarization P_{in} component, however, depends upon the QL stacking style. In $3R$ arrangement, it increases up to the trilayer system and thereafter it gradually weakens and eventually becomes smaller than P_{out} after the quad layer. On the other hand, in the $2H$ system, the P_{in} vanishes in an even number of layer structures and is nonzero in an odd number of layer structures because in this stacking arrangement each successive QL is a mirror image of its preceding QL in the xy plane [see Fig. 1(b)], therefore, P'_{in} components cancel themselves in the even number of QLs. Our theoretical calculation of polarization in single and the layered $3R$ and $2H$ structures of α-In$_2$Se$_3$ are in good

agreement with the results reported earlier. For instance, a similar trend of polarization in the layered $3R$ structure was earlier reported by Dai *et al.* [40] and Ding *et al.* [17] as calculated using Berry's phase method, while Cui *et al.* [25] reported an odd-even nature of in-plane polarization in the layered $2H$ structure.

Band structure and shift current — It is seen above that the ferroelectric properties of α-In$_2$Se$_3$ are sensitive to the nature of stacking of QLs, however, the electronic band profile of these structures is essentially similar, suggesting that the interlayer interaction is quite weak in nature [22,41]. A representative band structure of a single-layer α-In$_2$Se$_3$ is shown in Fig. 2(a). Single-layer α-In$_2$Se$_3$ is an indirect band gap semiconductor with conduction-band minimum (CBM) at the Γ point and the valance-band maximum (VBM) lies between the Γ and M points. The fat band of a QL [Fig. 2(b)] reveals that the $p_{x/y}$ orbitals of In$_{oc}$ (at octahedra site) and $p_{z/x}$ orbitals of In$_{tr}$ (at the tetrahedral site) form a degenerated orbital which combines with the p orbitals of Se$_{tg1}$ (at the top layer) and the p_z orbital of Se$_{tr}$ (at the tetrahedral site) to form the VBM, whereas the CBM is composed of the s orbital of In$_{tr}$ (at the tetrahedral site) hybridized with the p orbitals of Se$_{tg2}$ (at the bottom layer) and the p_z orbital of In$_{tr}$ (at the tetrahedral site).

We calculate the band gap with different methods (Table I) which match closely with the previous reports [17–19,43]. The USPP/LDA $+$ U ($U_{In} = 4.6$ eV, $U_{Se} = 4.6$ eV) band gap of α-In$_2$Se$_3$ matches very well with the band gap calculated using hybrid functional HSE06. The band structures of single-layer α-In$_2$Se$_3$, as calculated using LDA $+$ U and HSE06, are shown in Fig. S2 in the Supplemental Material [37]. Therefore, using the optimized LDA $+$ U Kohn Sham potentials, the MLWFs are further obtained. To perform the Wannierization, a frozen window of 14 eV is chosen to contain the low-energy region, whereas the outer window extends up to 24 eV to capture the manifold of 50 bands. For initial projections, we choose s and p trial orbitals of each atom. The LDA $+$ U and Wannier-interpolated energy bands are shown in Fig. 3. The Wannier interpolation is further extended to calculate shift current response in α-In$_2$Se$_3$ in the postprocessing step.

Following Ref. [11], we report 3D-like shift current response (σ) which is obtained by rescaling the response of the

TABLE I. Electronic band gaps of single-layer 3R α-In$_2$Se$_3$ calculated with different approaches. Results are also compared with previous reports.

Band gap	USPP/LDA + U	USPP/GGA + U	PAW/LDA + U	HSE06	Previous reports
Indirect (eV)	1.404	1.402	1.407	1.404	1.46[a] [17]
Direct (eV)	1.416	1.414	1.415	1.467	1.55[b] [42]

[a]Obtained with HSE06.

[b]Electronic band gap measured using high-resolution electron energy-loss spectroscopy (HR-EELS).

slab as $\sigma = $ (slab thickness/layer thickness) σ_{slab}. The shift current is calculated with the optimized k-point interpolation mesh obtained after performing the convergence test. With the k grid of $30 \times 30 \times 1$ in the non-self-consistent calculations, a well converged shift current spectrum of α-In$_2$Se$_3$ can be obtained by using the k-point interpolation mesh of $200 \times 200 \times 1$. On further increasing the k-point interpolation mesh, the shift current changes insignificantly (see Fig. S3 in the Supplemental Material [37]). Furthermore, the stability of shift current against different pseudopotentials is also examined (see Fig. S4 in the Supplemental Material [37]). Different pseudopotentials, USPP/LDA, USPP/GGA, and PAW/LDA, yield similar shift current response (with some qualitative differences mostly at the higher energy regions) with almost equal magnitude. Therefore, here we present the shift current response calculated using USPP/LDA. Besides, we successfully reproduce the previously reported shift current response of bulk GaAs and single-layer GeS [11] by the Wannier90 code which indicates the robustness of our calculations (see Figs. S5 and S6 in the Supplemental Material [37]).

The α-In$_2$Se$_3$ belongs to C_{3v} symmetry and has a mirror plane perpendicular to $\hat{x}$, leading to five independent nonvanishing shift current response tensors [44]: $Zxx = Zyy$, $Yyy = -Yxx = -Xxy = Xyx$, Zzz, $Xxz = Yyz$, and $Xzx = Yzy$, where the upper case letter represents the direction of shift current susceptibility and the last two lower case letters represent light polarization. For a monochromatic light linearly polarized along a particular direction, we calculate longitudinal (σ^{Zzz}, σ^{Yyy}) and transverse (σ^{Zyy}) shift current responses. The longitudinal component, σ^{Zzz} (σ^{Yyy}),

represents the shift current response along the Z (Y) axis, i.e., along the direction of out-of-plane (in-plane) polarization due to zz (yy) polarized light, whereas the transverse component σ^{Zyy} represents the shift current response along the Z axis due to yy polarized light.

The longitudinal and transverse shift current responses in a single-layer α-In$_2$Se$_3$ are shown in Fig. 4(a). Surprisingly, the shift current response σ^{Zzz} is the *only* dominant current
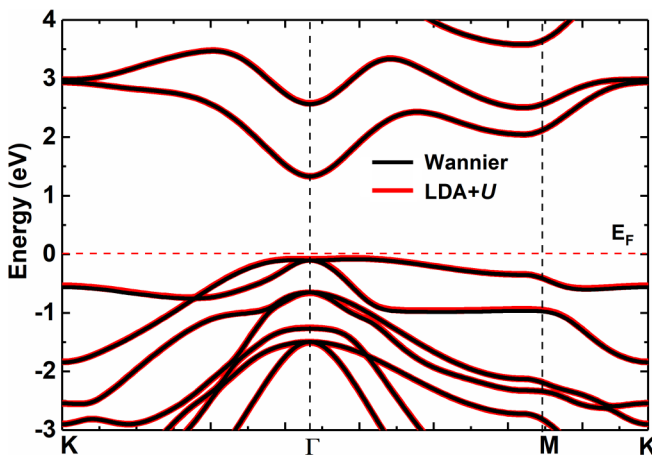

FIG. 4. (a) Longitudinal (σ^{Zzz}, σ^{Yyy}) and transverse (σ^{Zyy}) shift current responses in single-layer α-In$_2$Se$_3$. (b) Absorption of zz, yy, and xx polarized light in α-In$_2$Se$_3$. A dominant shift current response σ^{Zzz} along P_{out} under the illumination of zz-polarized light is indeed consistent with the larger absorption of zz-polarized light in α-In$_2$Se$_3$.

FIG. 3. LDA + U and Wannier-interpolated energy bands of monolayer α-In$_2$Se$_3$.

response in this material. In a QL of α-In$_2$Se$_3$ with a thickness of 6.8 Å, the σ^{Zzz} is strikingly large and is of the order of 750 μA/V^2 at a photon energy of 4.16 eV. Previously, the shift current of $\sim$50 μA/V^2 and $\sim$30 μA/V^2 was reported in the prototypical ferroelectrics PbTiO$_3$ and BaTiO$_3$, respectively [4], and that of $\sim$40 μA/V^2 was reported in the bulk GaAs [11] (see Fig. S5 in the Supplemental Material [37]). Additionally, in 2D materials, the shift current of $\sim$100 μA/V^2 is reported in single-layer GeS [8] (see Fig. S6 in the Supplemental Material [37]). Therefore, the shift current in α-In$_2$Se$_3$ is quite larger than that in the previously reported 3D bulk and 2D materials.

It is interesting to note in Fig. 4(a) that the σ^{Zzz} is only a dominant current response and σ^{Yyy} is nearly zero despite the fact that $P_{\text{out}} < P_{\text{in}}$ in single-layer α-In$_2$Se$_3$. This observation raises two questions: (i) Why is σ^{Zzz} the *only* dominant current response and the σ^{Yyy} component of the shift current is negligible? (ii) Is the shift current not influenced by P_{in} in this material? In order to understand the first question, we calculate the dielectric absorptive spectrum (imaginary dielectric constant, ε_{bb}^{im}) which is given as [11]

$$\varepsilon_{bb}^{im}(\omega) = \frac{i\pi e^2}{\hbar} \int [d\boldsymbol{k}] \sum_{n,m} f_{nm} r_{mn}^b r_{nm}^b \times \delta(\omega_{mn} - \omega). \quad (5)$$

The product of the last two terms in the right-hand side of Eq. (5), $r_{nm}^b r_{mn}^b \times \delta(\omega_{mn} - \omega) = |r_{nm}^b|^2 \delta(\omega_{mn} - \omega)$, represents the transition rate from band m to band n. From Eqs. (5) and (3) it is clear that the shift current depends upon the transition rate, therefore, it inherits most of its features from the absorption spectrum [4,8,11]. The absorption spectrum, shown in Fig. 4(b), indicates the highly anisotropic nature of α-In$_2$Se$_3$ which agrees well with the previous reports [36,45]. Higher absorption of zz-polarized light than the xx/yy-polarized light in single-layer α-In$_2$Se$_3$ is indeed consistent with the large σ^{Zzz} tensor response in this material. Previously, a similar trend was also reported in the single-layer GeS 2D material system [8,11]. It is to be noted in Fig. 4 that the maximum absorption of zz-polarized light and the corresponding shift current response along the Z axis, σ^{Zzz}, occur at $\sim$4.16 eV which approximately equals the energy separation between the upper valance band due to the Se p orbitals and the lower conduction band due to the In s orbital (see Fig. S7 in the Supplemental Material [37]). Clearly, the peak of shift current response lies well outside the visible spectrum [lies in the ultraviolet (UV) range]. However, for efficient solar conversion, the peak of shift current response in the visible spectrum is highly desired. Therefore, in the later section, we will discuss a mechanism by which the shift current response in α-In$_2$Se$_3$ can be brought inside the visible spectrum.

Now, coming back to understand the question (ii) that if the shift current is not influenced by P_{in} in single-layer α-In$_2$Se$_3$, it is interesting to note that the P_{in} is greater than P_{out}, but a negligible shift current is obtained along the direction of P_{in}. Although the strength and direction of polarization are not directly related to the shift current in any obvious ways, the maximum shift current response has been reported along the direction of polarization in many material systems (leaving few exceptions, e.g., BiFeO$_3$ [3]), including 2D materials. For example, in prototypical ferroelectrics, BaTiO$_3$, and PbTiO$_3$,
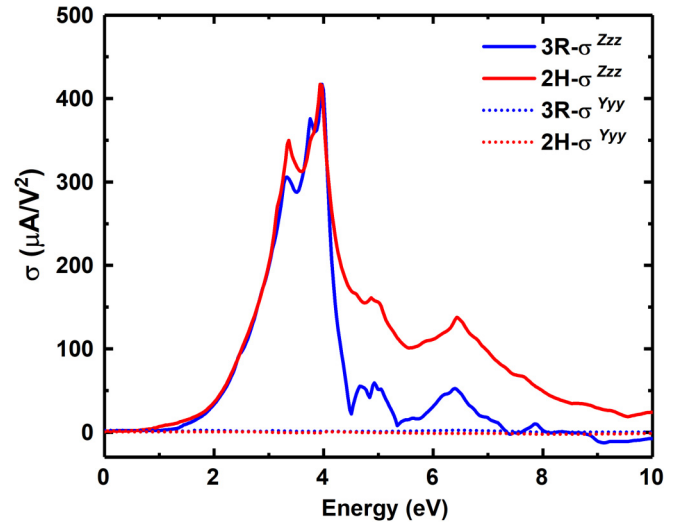

FIG. 5. Shift current in the bilayer of 3R and 2H α-In$_2$Se$_3$. The bilayer of 3R has both P_{out} and P_{in} whereas 2H has *only* P_{out} nonzero component. The σ^{Zzz} is *only* a dominant shift current in 3R and 2H α-In$_2$Se$_3$ along P_{out} under zz-polarized light, also σ^{Zzz} in 3R and 2H are equal in magnitude; this confirms that P_{in} doesn't affect shift current BPVE in α-In$_2$Se$_3$.

the bulk polarization and shift current are reported along the same direction [4]. Similar reports are also available for perovskite halide CH$_3$NH$_3$PbI$_3$ [16] and 2D material like GeS [8]. The α-In$_2$Se$_3$ material system, however, is one of its kind in which P_{in} and P_{out} coexist. The dominant shift current σ^{Zzz} along the direction of P_{out} [Fig. 4(a)] suggests that in-plane polarization has either no or less significance to the shift current in this material. In order to further confirm the influence of P_{in} on shift current, we calculate the shift current in bilayer 3R and 2H α-In$_2$Se$_3$ structures where in the former case there exist both P_{in} and P_{out} while in the latter structure there exists *only* P_{out} as explained above in Fig. 1. Remarkably, in both 3R and 2H α-In$_2$Se$_3$ bilayer structures, the σ^{Zzz} is *only* a dominant shift current response with almost equal magnitude as shown in Fig. 5. It is to be noted that to eliminate the spurious interlayer screening [46], the shift current in the bilayer is calculated using a vacuum level of 40 Å. The trend of shift current in mono- and bilayer structures confirms that the particular value of in-plane polarization (P_{in}) is insignificant in BPVE shift current in single-layer α-In$_2$Se$_3$; rather the symmetry breaking along with higher absorption spectrum is leading to the large shift current.

Shift current engineering via doping — It is clear from the above discussion that in single-layer α-In$_2$Se$_3$ the maximum BPVE shift current response can be achieved along the Z axis when illuminated by zz-polarized light. But the peak of shift current response lies well outside the visible spectrum in the ultraviolet range [Fig. 4(a)]. The peak of shift current response in the visible spectrum is highly desired for efficient solar energy conversion. Therefore, here in this section, we discuss a prototypical doping strategy by which the shift current response is tuned effectively for photovoltaic application under visible solar light.
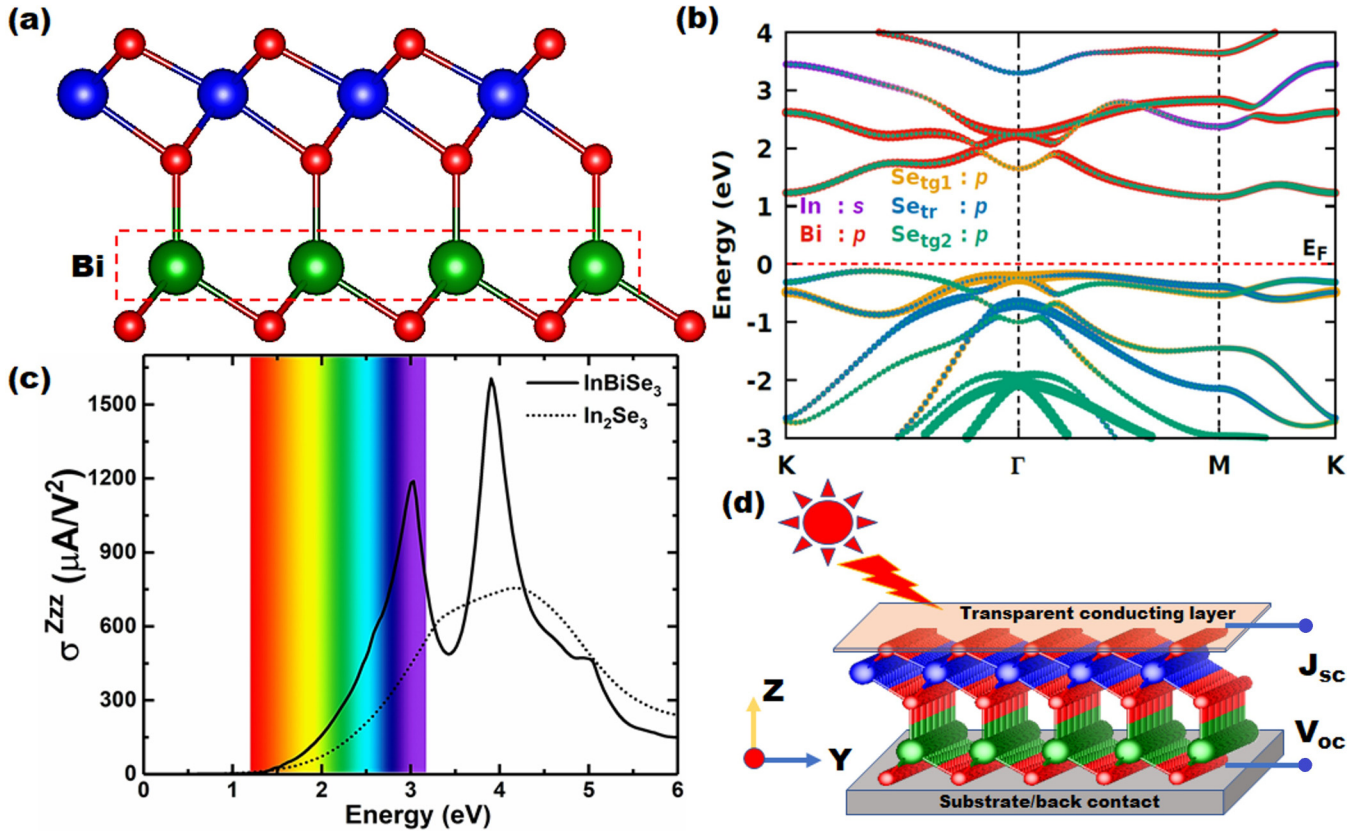
FIG. 6. Demonstrating doping engineering in a QL of α-In$_2$Se$_3$. (a) In$_{tr}$ at the tetrahedral site is substituted by Bi to obtain a QL of InBiSe$_3$ with $P_{in} = 0.391$ nC/m, and $P_{out} = 3.088$ nC/m; (b) fat band of QL of InBiSe$_3$ shows that the Bi substitution introduces more bands in CBM which importantly composed of p orbitals of Bi and Se. (c) Dominant shift current response in InBiSe$_3$ is along the direction of P_{out} under zz-polarized light. Two sharp peaks, one in the visible spectrum and another in the ultraviolet range, which is much higher than that in α-In$_2$Se$_3$, is obtained. (d) Proposed device model based on α-In$_2$Se$_3$ and InBiSe$_3$ material system.

It is well known that doping engineering is a key mechanism to modulate electronic [47], optical [48], magnetic [49], and many other exotic properties of 2D materials for different applications [41]. The ultrathin nature of 2D materials not only allows traditional substitutional doping strategies by implantation or diffusion processes, but also enables new methods such as surface charge transfer, intercalation, and field-effect modulation methods. Here we theoretically demonstrate the substitutional doping of the bismuth (Bi) element in a QL of α-In$_2$Se$_3$ which results in improving the shift current response under visible light in the resulting QL of InBiSe$_3$. Notably, the substitution of a foreign atom for any particular element in α-In$_2$Se$_3$ is a bit tricky in the sense that atoms are differently coordinated and substitution at a particular site may lead to an attribute suitable for a particular application.

As seen above in Fig. 4(a), the maximum shift current response σ^{Zzz} for the QL of α-In$_2$Se$_3$ occurs at 4.16 eV which approximately equals the energy separation between the upper valance band due to Se p orbitals and the lower conduction band due to In s orbital (see Fig. S7 in the Supplemental Material [37]). Therefore, increasing the density of states (DOS) near the CBM would enhance the transition rates under visible light and thereby modulate the shift current response. However, the increment of DOS should not be on account of the introduction of localized d orbitals as it may reduce the shift current response [12]. Therefore, we choose the bismuth (Bi)

element as it has half filled p orbitals ([Xe]$4f^{14}5d^{10}6s^26p^3$) which contribute to bands taking part in the transition process near the Fermi level. It is worth noting here that the CBM of α-In$_2$Se$_3$ is primarily contributed by the s orbital of In$_{tr}$ (at the tetrahedral site, Fig. 1); therefore, we substitute this indium element by Bi to obtain a QL of InBiSe$_3$, as shown in Fig. 6(a). Although the doping percentage considered in this study may be difficult to obtain experimentally, it serves a good example for demonstrating the doping engineering of shift current in α-In$_2$Se$_3$.

Single-layer InBiSe$_3$ is an indirect semiconductor with band gap 1.28 eV as obtained using the hybrid functional HSE06. The CBM lies at M and the VBM lies between Γ and M. Substitution of In$_{tr}$ with Bi introduces more bands in the CBM as shown in the fat bands of InBiSe$_3$ in Fig. 6(b). The CBM comprises Bi-p and Se$_{tg2}$-p orbitals and the VBM is not affected by Bi substitution. When illuminated under the zz-polarized light, a giant shift current (σ^{Zzz}) response of magnitude $\sim 1200\,\mu$V/cm^2 is obtained, which is almost double that of the QL of α-In$_2$Se$_3$ along the Z axis in the visible spectrum (at 2.98 eV) as shown in Fig. 6(c) (the transverse and longitudinal components of the shift current are shown in Fig. S8 in the Supplemental Material [37]). Thus, using doping engineering, the shift current response of α-In$_2$Se$_3$ can be modulated effectively to occur in the visible spectrum. Notably, the shift current response of InBiSe$_3$ contains two

sharp peaks, one at 2.98 eV (in the visible spectrum) and another at 3.89 eV (in the ultraviolet spectrum) suggesting that $InBiSe_3$ can generate a larger photocurrent in visible as well as ultraviolet light. It is worth mentioning here that we used both longitudinal and transverse polarized lights, however σ^{Zzz} is the dominant shift current response in the QL of $InBiSe_3$, indicating that a vertical device would be more efficient than a lateral device. Such a device model is schematically shown in Fig. 6(c) which can be realized easily using exfoliation [19] or chemical vapor deposition [20] techniques on a substrate (such as Si/SiO_2) with a conducting layer acting as a back contact. A transparent conducting layer (such as of indium tin oxide) can be deposited at the top which would allow the solar light to fall on to the $InBiSe_3$ layer. The maximum photogenerated charge carriers are collected via the transparent conducting layer at the top along the Z axis, thereby the maximum solar energy conversion efficiency can be obtained with such devices in this material system.

IV. CONCLUSION

α-In_2Se_3 is a 2D van der Waals layered material with in-plane and out-of-plane polarizations coexisting at room temperature. We calculate the shift current in this material to understand the implication of polarizations on BPVE. In a single layer, a larger shift current of $750\,\mu A/V^2$ at the photon energy of 4.16 eV is obtained along the direction of out-of-plane polarization under the illumination of zz-polarized light whereas a negligible shift current is obtained along the direction of in-plane polarization under yy-polarized light. Furthermore, in the bilayer, a dominant shift current along the direction of out-of-plane polarization is obtained in both $3R$ and $2H$ arrangement, confirming that in-plane polarization doesn't affect the shift current in α-In_2Se_3.

Moreover, we have found that the maximum shift current response occurs in the ultraviolet energy range in this material. Therefore, for efficient solar energy conversion, the shift current is tuned to the visible spectrum by doping engineering. The indium element at the tetrahedral site is substituted by bismuth, thereby a giant shift current response of $1200\,\mu A/V^2$ is obtained at 2.98 eV in the resulting composition, $InBiSe_3$, under zz-polarized visible light along the direction of out-of-plane polarization. This study would be instrumental in understanding the BPVE in α-In_2Se_3 and similar material systems. A device model is also proposed which would guide design of an efficient solar energy converter based on this material.

[1] V. M. Fridkin, Crystallogr. Rep. **46**, 654 (2001).

[2] S. Y. Yang, J. Seidel, S. J. Byrnes, P. Shafer, C. H. Yang, M. D. Rossell, P. Yu, Y. H. Chu, J. F. Scott, J. W. Ager, L. W. Martin, and R. Ramesh, Nat. Nanotechnol. **5**, 143 (2010).

[3] S. M. Young, F. Zheng, and A. M. Rappe, Phys. Rev. Lett. **109**, 236601 (2012).

[4] S. M. Young and A. M. Rappe, Phys. Rev. Lett. **109**, 116601 (2012).

[5] A. M. Cook, B. M. Fregoso, F. De Juan, S. Coh, and J. E. Moore, Nat. Commun. **8**, 14176 (2017).

[6] R. P. Tiwari, B. Birajdar, and R. K. Ghosh, J. Phys.: Condens. Matter **31**, 505502 (2019).

[7] B. M. Fregoso, Phys. Rev. B **100**, 064301 (2019).

[8] T. Rangel, B. M. Fregoso, B. S. Mendoza, T. Morimoto, J. E. Moore, and J. B. Neaton, Phys. Rev. Lett. **119**, 067402 (2017).

[9] J. E. Sipe and A. I. Shkrebtii, Phys. Rev. B **61**, 5337 (2000).

[10] C. Wang, X. Liu, L. Kang, B. L. Gu, Y. Xu, and W. Duan, Phys. Rev. B **96**, 115147 (2017).

[11] J. Ibañez-Azpiroz, S. S. Tsirkin, and I. Souza, Phys. Rev. B **97**, 245143 (2018).

[12] L. Z. Tan, F. Zheng, S. M. Young, F. Wang, S. Liu, and A. M. Rappe, NPJ Comput. Mater. **2**, 16026 (2016).

[13] S. R. Basu, L. W. Martin, Y. H. Chu, M. Gajek, R. Ramesh, R. C. Rai, X. Xu, and J. L. Musfeldt, Appl. Phys. Lett. **92**, 091905 (2008).

[14] Z. Chen, Y. Wang, D. Zheng, F. Sun, X. Deng, Z. Tan, J. Tian, L. Zhang, M. Zeng, Z. Fan, D. Chen, Z. Hou, X. Gao, Q. Li, and J. Ming Liu, J. Alloys Compd. **811**, 152013 (2019).

[15] L. You, F. Zheng, L. Fang, Y. Zhou, L. Z. Tan, Z. Zhang, G. Ma, D. Schmidt, A. Rusydi, L. Wang, L. Chang, A. M. Rappe, and J. Wang, Sci. Adv. **4**, eaat3438 (2018).

[16] F. Zheng, H. Takenaka, F. Wang, N. Z. Koocher, and A. M. Rappe, J. Phys. Chem. Lett. **6**, 31 (2015).

[17] W. Ding, J. Zhu, Z. Wang, Y. Gao, D. Xiao, Y. Gu, Z. Zhang, and W. Zhu, Nat. Commun. **8**, 14956 (2017).

[18] L. Hu and X. Huang, RSC Adv. **7**, 55034 (2017).

[19] P. Hou, Y. Lv, X. Zhong, and J. Wang, ACS Appl. Nano Mater. **2**, 4443 (2019).

[20] R. B. Jacobs-Gedrim, M. Shanmugam, N. Jain, C. A. Durcan, M. T. Murphy, T. M. Murray, R. J. Matyi, R. L. Moore, and B. Yu, ACS Nano **8**, 514 (2014).

[21] M. Küpers, P. M. Konze, A. Meledin, J. Mayer, U. Englert, M. Wuttig, and R. Dronskowski, Inorg. Chem. **57**, 11775 (2018).

[22] F. Xue, W. Hu, K. C. Lee, L.S. Lu, J. Zhang, H. L. Tang, A. Han, W. T. Hsu, S. Tu, W. H. Chang, C. H. Lien, J. H. He, Z. Zhang, L. J. Li, and X. Zhang, Adv. Funct. Mater. **28**, 1803738 (2018).

[23] F. Xue, J. Zhang, W. Hu, W.T. Hsu, A. Han, S. F. Leung, J. K. Huang, Y. Wan, S. Liu, J. Zhang, J. H. He, W. H. Chang, Z. L. Wang, X. Zhang, and L. J. Li, ACS Nano **12**, 4976 (2018).

[24] T. Zhai, X. Fang, M. Lio, X. Xu, B. Li, Y. Koide, Y. Ma, J. Yao, Y. Bando, and D. Golberg, ACS Nano **4**, 1596 (2010).

[25] C. Cui, W. J. Hu, X. Yan, C. Addiego, W. Gao, Y. Wang, Z. Wang, L. Li, Y. Cheng, P. Li, X. Zhang, H. N. Alshareef, T. Wu, W. Zhu, X. Pan, and L. J. Li, Nano Lett. **18**, 1253 (2018).

[26] P. Giannozzi, S. Baroni, N. Bonini, M. Calandra, R. Car, C. Cavazzoni, D. Ceresoli, G. L. Chiarotti, M. Cococcioni, I. Dabo, A. Dal Corso, S. de Gironcoli, S. Fabris, G. Fratesi, R. Gebauer, U. Gerstmann, C. Gougoussis, A. Kokalj, M. Lazzeri, L. Martin-Samos, N. Marzari, F. Mauri, R. Mazzarello, S. Paolini, A. Pasquarello, L. Paulatto, C. Sbraccia, S. Scandolo,

G. Sclauzero, A. P. Seitsonen, A. Smogunov, P. Umari, and R. M. Wentzcovitch, J. Phys.: Condens. Matter **21**, 395502 (2009).

[27] D. Vanderbilt, Phys. Rev. B **41**, 7892 (1990).

[28] J. P. Perdew and A. Zunger, Phys. Rev. B **23**, 5048 (1981).

[29] E. R. Davidson, J. Comput. Phys. **17**, 87 (1975).

[30] I. V. Lebedeva, A. V. Lebedev, A. M. Popov, and A. A. Knizhnik, Comput. Mater. Sci. **128**, 45 (2017).

[31] J. Klimeš, D.R. Bowler, and A. Michaelides, J. Phys.: Condens. Matter **22**, 022201 (2010).

[32] R. D. King-Smith and D. Vanderbilt, Phys. Rev. B **47**, 1651 (1993).

[33] K. Hummer, J. Harl, and G. Kresse, Phys. Rev. B **80**, 115205 (2009).

[34] S. Smidstrup, T. Markussen, P. Vancraeyveld, J. Wellendorff, J. Schneider, T. Gunst, B. Verstichel, D. Stradi, P. A. Khomyakov, U. G. Vej-Hansen, M.-E. Lee, S.T. Chill, F. Rasmussen, G. Penazzi, F. Corsetti, A. Ojanperä, K. Jensen, M. L. N. Palsgaard, U. Martinez, A. Blom *et al.*, J. Phys.: Condens. Matter **32**, 015901 (2020).

[35] G. Pizzi, V. Vitale, R. Arita, S. Blügel, F. Freimuth, G. Géranton, M. Gibertini, D. Gresch, C. Johnson, T. Koretsune, J. Ibañez-Azpiroz, H. Lee, J. M. Lihm, D. Marchand, A. Marrazzo, Y. Mokrousov, J. I. Mustafa, Y. Nohara, Y. Nomura, L. Paulatto *et al.*, J. Phys.: Condens. Matter **32**, 165902 (2020).

[36] D. Wu, A. J. Pak, Y. Liu, Y. Zhou, X. Wu, Y. Zhu, M. Lin, Y. Han, Y. Ren, H. Peng, Y. H. Tsai, G. S. Hwang, and K. Lai, Nano Lett. **15**, 8136 (2015).

[37] See Supplemental Material at http://link.aps.org/supplemental/10.1103/PhysRevB.101.235448 for coordination polyhedra,

band structure optimization, and shift current optimization in single-layer α-In$_2$Se$_3$.

[38] S. Shen, C. Liu, Y. Ma, B. Huang, and Y. Dai, Nanoscale **11**, 11864 (2019).

[39] Z. Liu, Y. Sun, D. J. Singh, and L. Zhang, Adv. Electron. Mater. **5**, 1900089 (2019).

[40] M. Dai, Z. Wang, F. Wang, Y. Qiu, J. Zhang, C. Y. Xu, T. Zhai, W. Cao, Y. Fu, D. Jia, Y. Zhou, and P. A. Hu, Nano Lett. **19**, 5410 (2019).

[41] P. Luo, F. Zhuge, Q. Zhang, Y. Chen, L. Lv, Y. Huang, H. Li, and T. Zhai, Nanoscale Horizons **4**, 26 (2019).

[42] S. M. Poh, S. J. R. Tan, H. Wang, P. Song, I. H. Abidi, X. Zhao, J. Dan, J. Chen, Z. Luo, S. J. Pennycook, A. H. Castro Neto, and K. P. Loh, Nano Lett. **18**, 6340 (2018).

[43] R. Peng, Y. Ma, S. Zhang, B. Huang, L. Kou, and Y. Dai, Mater. Horizons **7**, 504 (2020).

[44] R. W. Boyd, *Non-Linear Optics*, 3rd ed. (Elsevier, New York, 2008).

[45] H. Peng, C. Xie, D. T. Schoen, and Y. Cui, Nano Lett. **8**, 1511 (2008).

[46] F. Hüser, T. Olsen, and K. S. Thygesen, Phys. Rev. B **88**, 245309 (2013).

[47] H. Schmidt, F. Giustiniano, and G. Eda, Chem. Soc. Rev. **44**, 7715 (2015).

[48] Y. Zhao, K. Xu, F. Pan, C. Zhou, F. Zhou, and Y. Chai, Adv. Funct. Mater. **27**, 1603484 (2017).

[49] V. Kochat, A. Apte, J. A. Hachtel, H. Kumazoe, A. Krishnamoorthy, S. Susarla, J. C. Idrobo, F. Shimojo, P. Vashishta, R. Kalia, A. Nakano, C. S. Tiwary, and P. M. Ajayan, Adv. Mater. **29**, 1703754 (2017).